

TITLE: SUPERCONDUCTOR DESIGN AND LOSS ANALYSIS FOR A 20 MJ INDUCTION HEATING COIL

AUTHOR(S): M. S. Walker, J. G. Declercq, B. A. Zeitlin, J. D. Scudiere, and M. J. Ross, Intermagnetics General Corporation; M. A. Janocko, S. K. Singh, E. Ibrahim, and P. W. Eckels, Westinghouse Electric Corporation; ^{THIS DOCUMENT} J(ohn) D. Rogers, and J(ohn) J. Wollan, CTR-S

SUBMITTED TO: Applied Superconductivity Conference,
Santa Fe, NM, September 20-October 3, 1980

MASTER

DISCLAIMER

This book was prepared as an account of work sponsored by an agency of the United States Government. Neither the United States Government nor any agency thereof, nor any of their employees, makes any warranty, expressed or implied, or assumes any legal liability or responsibility for the accuracy, completeness, or usefulness of any information, apparatus, product, or process disclosed, or represents that its use would not infringe privately owned rights. Reference herein to any specific commercial product, process, or service by trade name, trademark, manufacturer, or otherwise, does not necessarily constitute or imply its endorsement, recommendation, or approval by the United States Government or any agency thereof. The views and opinions of authors expressed herein do not necessarily state or reflect those of the United States Government or any agency thereof.

By acceptance of this article, the publisher recognizes that the U.S. Government retains a nonexclusive, royalty-free license to publish or reproduce the published form of this contribution, or to allow others to do so, for U.S. Government purposes.

The Los Alamos Scientific Laboratory requests that the publisher identify this article as work performed under the auspices of the U.S. Department of Energy.

DISTRIBUTION OF THIS DOCUMENT IS UNLIMITED

LOS ALAMOS SCIENTIFIC LABORATORY

Post Office Box 1683 Los Alamos, New Mexico 87545

An Affirmative Action/Equal Opportunity Employer

University of California



SUPERCONDUCTOR DESIGN AND LOSS ANALYSIS FOR A 20 MJ INDUCTION HEATING COIL,* M. S. Walker, J. G. Declercq, B. A. Zeitlin, J. D. Scudiere, and M. J. Ross, Inter-magnetics General Corporation; M. A. Janocko, S. K. Singh, E. Ibrahim, and P. W. Eckels, Westinghouse Electric Corporation; and J. D. Rogers and J. J. Wollan, Los Alamos Scientific Laboratory.

Summary

The design of a 50 k Ampere conductor for use in a 20 MJ Induction Heating Coil is described. The conductor is a wide flat cable of 36 subcables, each of which contains six NbTi strands around a stainless steel core strand. The 2.04 mm (0.080") diameter monolithic strands allow bubble clearing for cryo-stable operation at a pool boiling heat transfer from the unoccluded strand surface of 0.26 Watts/cm^2 . A thin, tough polyester amide-imide (Westinghouse Omega) insulation provides a rugged coating that will resist flaking and chipping during the cabling and compaction operations and provide (1) a reliable adherent surface for enhanced heat transfer, and (2) a low voltage standoff preventing interstrand coupling losses. The strands are uniquely configured using CuNi elements to provide low AC losses with NbTi filaments in an all-copper matrix. AC losses are expected to be approximately 0.3% of 20 MJ for a -7.5 T to 7.5 T one-second 1/2-cosinusoidal bipolar operation in a 20 MJ coil. They will be approximately 0.1% of 100 MJ for 1.8 second -8 T and +8 T ramped operation in a 100 MJ coil. The design is firmly based on the results of tests performed on prototype strands and subcables.

*Supported by the University of California, Los Alamos Scientific Laboratory Contract No. 4-XP9-3459H-1.

I. Introduction

In anticipation of the probable need for a superconducting ohmic heating coil for experimental Tokamak devices and reactors, the Department of Energy has funded a Westinghouse/IGC team with guid-

ance from the Los Alamos Scientific Laboratory to design and construct a 20 MJ induction heating coil. The detailed design of this coil has now been completed⁽¹⁾, and a summary description of the design is presented in a companion paper⁽²⁾. The manufacturing phase of the 20 MJ coil program has begun. A fundamental part of the design was the choice of conductor concept and conductor design and analysis, including the analysis of conductor losses and stability. This paper presents the conductor design, and supporting analyses, with reference to related design choices and prototype conductor strand and cable development and testing.

II. The Conductor/Coil Design Problem and Westinghouse/IGC Approach

For the 20 MJ coil LASL specified a pool boiling cryostable conductor for operation with the approximate field change, 15 Tesla (-7.5 T to +7.5 T) and minimum pulse time, one second, that is likely for a TNS or BTF device. The design must also include a mechanical strength and ruggedness appropriate to 10^5 pulse cycles of the coil.

To maximize the flux produced by the OH coil, a relatively thin, high current density winding is desirable. However, the conductor must be subdivided into small elements to reduce the AC losses that are produced during the induction heating pulse, and subdivision of the conductor is otherwise recommended to create surface for heat transfer to meet the specification of cryostability. Sufficient winding stiffness must be retained, however, to prevent losses due to mechanical hysteresis, and the coil must be self supported with a low loss structure.

The Westinghouse/IGC approach has been to provide the long lifetime and integrity normally associated with the electrical utility industry. A pancake-wound coil approach has been ~~taken~~^{chosen}, utilizing primarily G-10 structural materials to support axial

loads. As a starting point for the conductor design, wide, flat conductor to contain or be co-wound with steel reinforcements to accommodate the hoop load was determined⁽²⁾. For the conductor design, emphasis has been on the selection of a strand concept that allows the application of thin, tough insulations that will not degrade over the operating lifetime of the Tokomak machine. While losses have been reduced to manageable and acceptable levels, possible lower-loss designs were rejected in favor of ruggedness and reliability.

III. Conductor Design

The 20 MJ conductor is shown in Figure 1. To maximize winding current density the steel is enclosed as the core strap of a cable of subcables. This core, which supports the coil hoop load, was made as thin as possible through the utilization of a high strength Nitronic 40 stainless steel. The number of subcables was set at 36, the maximum number accommodated by conventional cabling machinery. The dimensions of the cable result from a selection of the smallest subcable strands possible, within the constraint that the operating current of 50,000 Amperes be achieved with the assurance of recovery from a fully-normalized long section of conductor. Each subcable consists of six Omega (polyester amide-imide) film-insulated monolithic superconductor strands cabled around a similarly insulated stainless steel core strand. A description of operating characteristics, component materials, parameters and dimensions of the cable and subcable is provided in Table 1. A description of the superconductor strand is provided in Table 2 with reference to the parameters defined in Figure 2.

The design of the superconductor strands proceeded through an interactive process consisting of (1) prototype strand design and manufacture, (2) initial 20 MJ strand design, (3) final sizing of the

prototype strands to represent very closely the 20 MJ design, (4) test of the prototype strands, (5) variation of prototype strand twist pitch length and retest as strand and subcable, and (6) alteration of the 20 MJ strand design to incorporate the test results. As a consequence, the 20 MJ strand design is firmly based on the direct measurement of strand parameters for prototype conductors of the 20 MJ design size and of the 20 MJ design configuration. A prototype of the 50 kAmp cable has subsequently been manufactured and delivered for testing.

The NbTi cross-section was established on the basis of critical current density measured in Prototype #1 and the choice of $0.71 I_{op}/I_c$ margin. The strand configuration was selected as part of a trade-off study that evaluated soldered-together cabled strands of smaller substrands⁽⁵⁾ as well as mixed matrix monolithic strands⁽⁶⁾ with copper-nickel~~separating~~ separating copper-sleeved filaments. The selected design combines the most efficient use of space for superconductor and stabilizer with the avoidance of solder, which would prevent the use of thin, strong reliable cured insulations. The copper-nickel thin ring and fins reduce the losses to desirable levels, although not to the levels that are possible with the cables of substrands or mixed matrix designs. The final strand size was adjusted to provide a fully-normal heat flux of 0.26 Watts/cm^2 from the unoccluded strand surface, assumed to be $1/23$ of the total strand surface. For this calculation, magnetoresistance was estimate from a zero field residual resistivity ratio of 90 ($273 \text{ K}/4.2 \text{ K}$) for the core matrix copper surrounding the filaments. The remainder of the copper was assumed to have a zero field RRR of 125. These values are based upon experimental test results on the prototype strands which show that the effective resistivity ratio of high purity OFHC copper of initial RRR greater than 150 is reduced to these

levels for the finned composite, with filaments of approximately the size and distribution of this 20 MJ design⁽³⁾. Values of resistivity at 4.5 K, 7.5 T of $4.9 \times 10^{-8} \Omega\text{-cm}$ and $4.7 \times 10^{-8} \Omega\text{-cm}$ were calculated for the two regions. The electrical conduction of the strands was found in tests on Prototype #2 to be essentially unchanged with twist to the degree specified in this design, while AC losses were substantially reduced.

The 2 mm diameter strand provides interstitial spaces and channels between crossing strands in adjacent subcables that are large enough to clear bubbles, based upon (1) the operation of the 540 kilojoule coil which required passages of this approximate size and (2) observations of boiling helium. The adequacy of bubble clearing will be tested in the 50 K amp prototype cable. The choice and thickness of insulation for the strands directly affects the strand performance. While it is desirable to make the insulation thin and of high thermal conductivity to prevent excessive temperature rise within the strand during recovery, it must adhere tightly to the strands and not flake or crack during cabling, winding, and operation. The major concern is not that the electrical insulation be damaged, since only low turn-to-turn, subcable-to-subcable and strand-to-strand voltages are encountered, where some shorts may be tolerated. It is that the insulation should provide a nearly complete voltage stand-off to prevent major coupling and losses, while adhering well enough so as not to loosely cover strand surfaces as an interference with helium movement and heat transfer. Polyester amide-imide insulation has been identified as tough and strongly adhering⁽⁴⁾. Tests of this insulation on the prototype strands have shown that it provides an adequate toughness and adherence for the low voltage electrical insulation needs of this design.⁽³⁾

Because of the twist pitch in the subcable, the strands will have an elliptical shape when sectioned normal to the subcable axis. The central strand of the subcable is thus larger than the strands for tight subcable packing. To avoid coupling between the central strand and the outside strands, which would result in large self-field losses for the cable and uneven current distribution, the central strand of the subcable is inactive and of relatively high resistivity to reduce eddy current losses. Type 304L stainless steel was selected because of its availability and its low temperature ductility and resistivity. A target cable pitch angle of 18° was determined to be suitable based upon IGC experience in previous cabling operations. The manufacture of the 50 kAmp prototype cable has confirmed that cabling around a wide thin flat core is achievable and most easily accomplished if the subcables are cabled about the core in the same direction and with the same sense of rotation experienced by the strands about the core of the subcable. The thickness of the stainless steel center of the core strap has been set by the structural requirement that it take up the hoop tension of the coil. The insulation scheme for this wide flat mandrel was selected on the basis of Westinghouse experience on the 540 kilojoule and 400 kilojoule METS coils. A b-stage epoxy-filled fiberglass tape is first wrapped around the mandrel, butt-lapped turn-to-turn. This wrap is followed by a thin layer of Kapton wrapped over the seams in the epoxy fiberglass, again butt-lapped. That layer is followed by a second layer of Kapton, butt-lapped in such a way that the seams in the prior Kapton layer are covered. The width of the insulated mandrel, w , has been determined on the basis of IGC experience with cables and the following approximate analysis, where the cable is considered to be composed of a series of $N=36$ ellipses of width $(\frac{d + \Delta d}{\cos \theta})$ side-by-side and wrapped around the cable mandrel (thickness

t and width w) and spanning the locus of subcable centers. θ is the cable pitch angle, d the subcable diameter, and Δd an effective added space required (normally about 2% of d) in cabling.

$$w \approx \frac{N(d + \Delta d)}{2} \left[\frac{1}{1 - \frac{N(d + \Delta d)^2}{2\ell}} \right]^{\frac{1}{2}} - \frac{\pi}{2} (t + d) + t$$

The cable will be made by cabling all 36 subcables through appropriate spider dies and feeding guides with a final in-line draw through a set of rollers which compacts the cable to the required flat shape, deforming the subcables at the cable edges to provide a set that maintains the cable shape. There will be considerable springback even after this compaction; the dimensions shown in Table 1 are therefore for the cable as tightly wound and axially and radially compressed in the winding, with the springback thus entirely removed.

IV. AC Losses for the 20 MJ Coil

The specifications for this program state that the total bipolar loss from all sources shall be targeted at less than 0.3% of 20 MJ where the coil is treated as a centrally located equivalent coil in a TNS long ohmic-heating solenoid, and that this target specification may be exceeded marginally with LASL approval for copper matrix strands. In particular, if a copper matrix conductor is utilized, then the 0.3% loss criterion may be met for two-second bipolar operation, provided it is not substantially exceeded for one-second bipolar operation. The operating losses for the coil can arise from two sources: (1) AC losses generated in the metallic components of the winding, and (2) mechanical hysteresis losses resulting from frictional and otherwise inelastic movement within the coil. The mechanical losses are not readily calculable and will eventually be determined by deduction from the measurement of losses

during operation of the 20 MJ coil. However, the elements of the cable have been made as large as possible, in part to provide a stiff and tight winding to limit these losses as much as possible while adhering to the remainder of the program specifications.

The central section of the TNS ohmic heating coil experiences a magnetic field environment approximating that of an infinitely long solenoid. Calculations for comparison with the 20 MJ coil specifications have therefore been performed in this approximation, where radial and azimuthal components of magnetic field change are zero. For the uniform winding of this 20 MJ design, the field strength increases from zero in proportion to the winding build from the outside to the inside diameter. The superconductor strands and metallic structural components of the coil thus experience losses from the one-second half cycle cosinusoidal transverse field change in relation to this distribution of peak fields. For comparison with anticipated test results ~~the coil operating alone with~~ AC losses have also been calculated for the same one second -50 kAmp to +50 kAmp pulse. The formulae used to calculate the various components of the loss and the losses calculated for both modes of coil operation are shown in Table 3. Since the currents responsible for these loss components usually tend to interfere in a way that reduces the total loss, the sums of the losses shown can be considered maxima. The distribution of total losses versus coil radius for these two cases is shown in Figure 3. The losses summarized in the Table can be divided into two classes, (1) the hysteretic losses which are independent of bipolar pulse time, and (2) eddy current and coupling losses which are inversely proportional to the pulse time. Generally, true hysteretic losses are independent of pulse time, and for the pulse times considered here, the fully-coupled parallel field

loss is hysteretic. The eddy current and coupling losses which comprise over 60% of the losses shown are inversely proportional to pulse time, and accordingly can be substantially reduced for longer pulse times. Although the primary objective of 0.3% loss for the coil operating in a stack for a one second pulse is marginally exceeded, the ~~projected~~^{calculated} 0.26% loss for a two second pulse meets the alternate program objective for copper matrix conductors. Note that the loss levels shown pertain specifically to the 20 MJ coil. Substantially different losses will be projected as a percent of coil energy for the same conductor operated with different current margins in coils of different sizes, as discussed in Section VI.

V. Thermohydraulic Analysis

Stability

The critical region with respect to stability in this ungraded winding is clearly at the bore of the coil at peak magnetic field. An assessment of the thermal environment for conductor turns in this region during the bipolar pulse shows the rate of heat generation within the conductor strands to be a maximum at the midpoint of the bipolar swing, with a corresponding maximum temperature in the strands as shown in Figure 4. The current sharing temperature, which is a function of magnetic field, shows a pronounced maximum at the same time, however. Thus, the worst-case situation with respect to stability occurs at peak field immediately subsequent to the pulse when conductor strands rest at 4.5°K and residual bubbles from the AC losses have maximum interference with helium replenishment for stabilization. If all of the losses were to result in the displacement of liquid helium, a gas fraction of 36.1% would be present after the pulse. Since the gas velocity from the conductor is expected to be faster than the liquid velocity, the liquid displacement is expected to be ~20% or less. Thus the thermal environment

just after the pulse is not excessively disturbed by the losses that occur, and a recovery analysis can be pursued in the standard fashion. It is interesting to note that the 540 kiloJoule coil, which was designed for a 50% gas fraction after pulsing, was normalized only after driving it beyond I_c at a current density ~~was~~ far in excess of cryostable limits.

Figure 5 shows the projected curve for heat removal for the 20 MJ strands, including the effects of the thin polyamide-imide insulation. The heat generation curve is almost entirely below the heat removal curve, indicating nearly unconditional recovery of the conductor strands. Very rapid propagation towards the center of the normal region from the cold ends is projected, producing a very nearly uniform and rapid cooling of the conductor throughout the normalized length. The conductor is thus conservatively cryostable. Experiments thus far on heat transfer with the thin polyamide-imide insulation on strand and subcables indicate that the predicted recovery will be achieved.

Protection

During the bipolar pulse, and possibly for reasons of control, before and after the pulse, large inductive voltages are experienced across the coil terminals. If it is desired that protective mechanisms be triggered in the event of quench, then the discrimination of low resistive voltages amongst large inductive potentials may be required. A protection scheme has been devised to handle this problem, as described in a companion paper⁽⁷⁾.

VI. Affect of Heat Transfer and Coil Size on % Loss

The losses reported in Section IV are for the 20 MJ coil, conservatively designed as described in this paper. Since increased heat transfer would allow a reduction in stabilizer volume the loss depends strongly upon the expected heat transfer. In

particular, for the 20 MJ strand where substantial margin in I_{op} relative to I_c has been allowed, the number of strands in the cable and the losses can be reduced in inverse proportion to the surface heat transfer. In the first three rows of Table 4 the conductor for the 20 MJ coil is shown in comparison with 50 kiloampere conductors using fewer strands identical to those of the 20 MJ design in inverse proportion to the surface heat transfer. Heat transfers of (1) 0.53 Watts/cm^2 , the value achieved in tests of Omega-insulated single prototype strands⁽³⁾, and (2) 0.36 Watts/cm^2 , a reasonable but more optimistic projection of achievable heat transfer from the cable, are considered, resulting in losses of $<0.22\%$ and $<0.26\%$ of 20 MJ, respectively. If the same conductor is used in a larger diameter coil, for the same peak field the winding thickness becomes a smaller fraction of the coil diameter, a lower % of conductor volume is therefore utilized, and the loss is reduced as a percentage of coil stored energy. A $<.1\%$ loss is projected, for example, for a 100 MJ coil of a 50 kiloampere conductor using 174 20-MJ strands in a -7.9 T to $+7.9 \text{ T}$ ramped field change in 1.8 seconds as shown in the last row of the Table.

VII. Conclusions

A conservative detailed conductor design for the 20 MJ coil has been produced in conjunction with a strongly interactive program of prototype fabrication and testing. The conductor meets all program specifications, with particular emphasis on achieving ruggedness, structural soundness, and insulation integrity over the 10^5 cycles anticipated for a Tokamak induction heating coil.

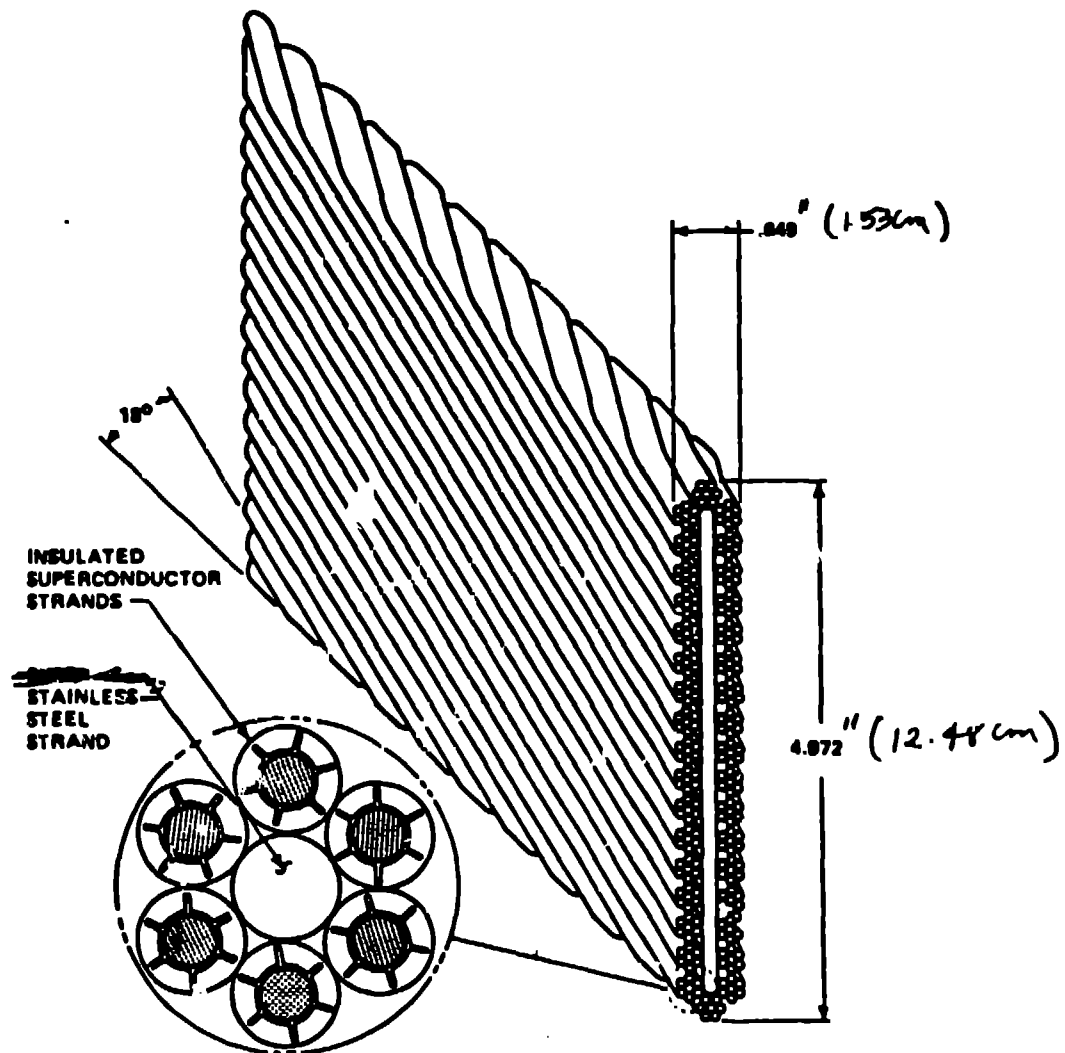
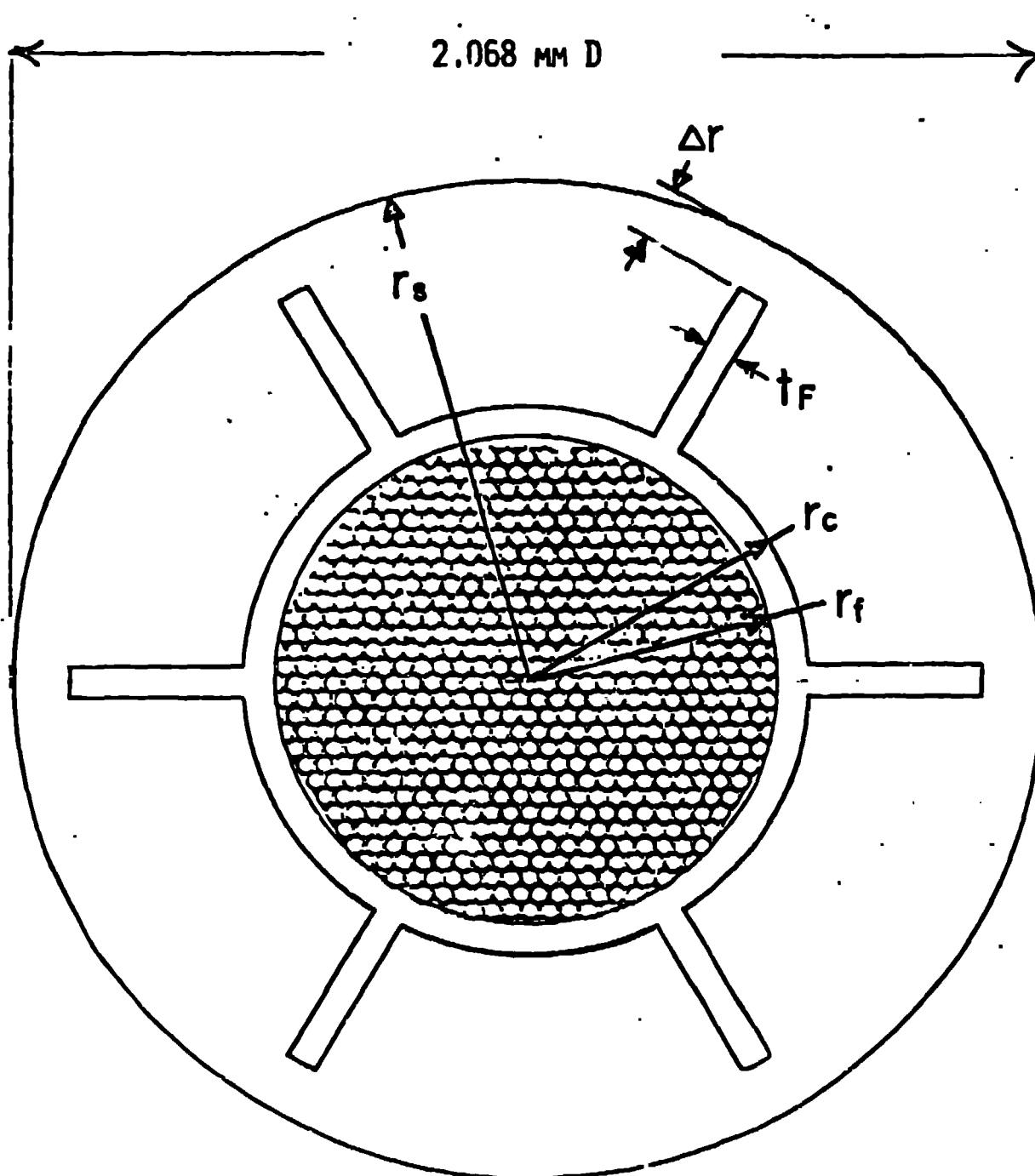
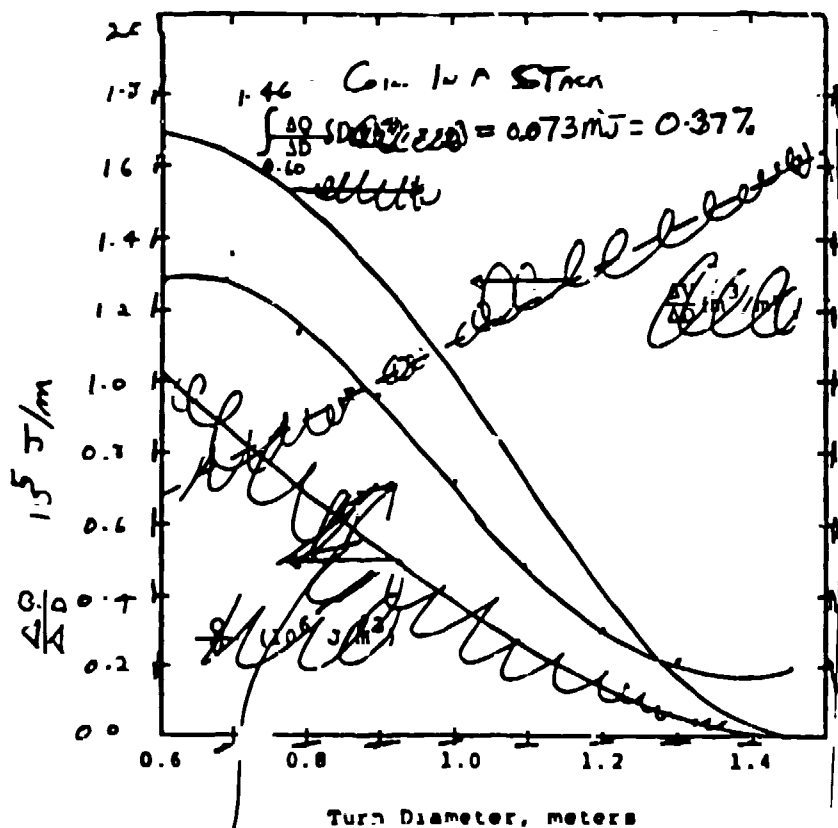


FIGURE 1 20 MJ SUPERCONDUCTING CABLE



INTERMAGNETICS ~~RESEARCH~~

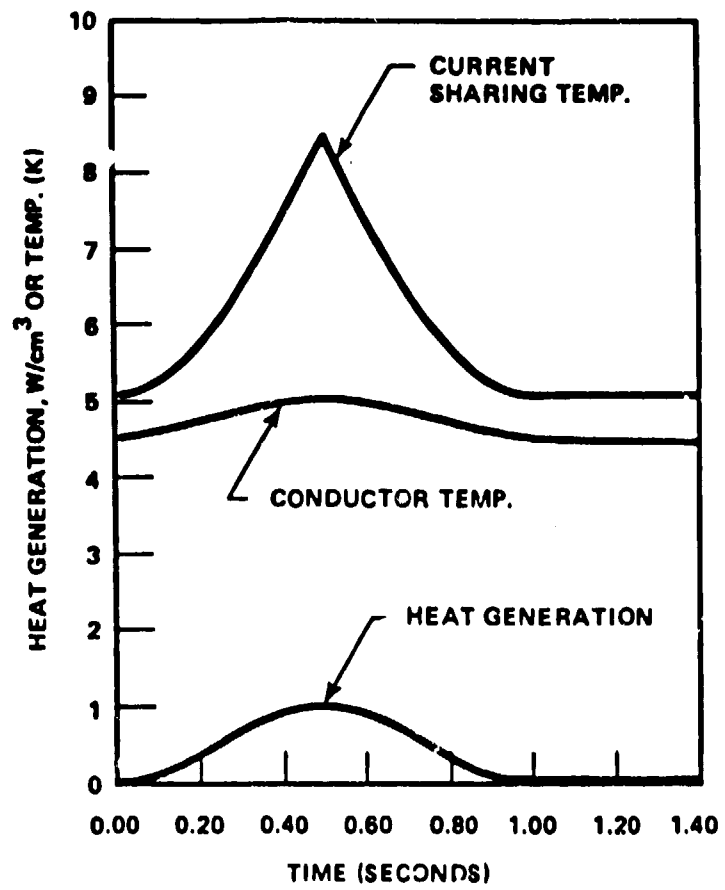
Figure 2 ~~2.1~~ Definition of strand parameters for composite of copper matrix NbTi surrounded by CuNi ring and fins separating outer copper annulus.



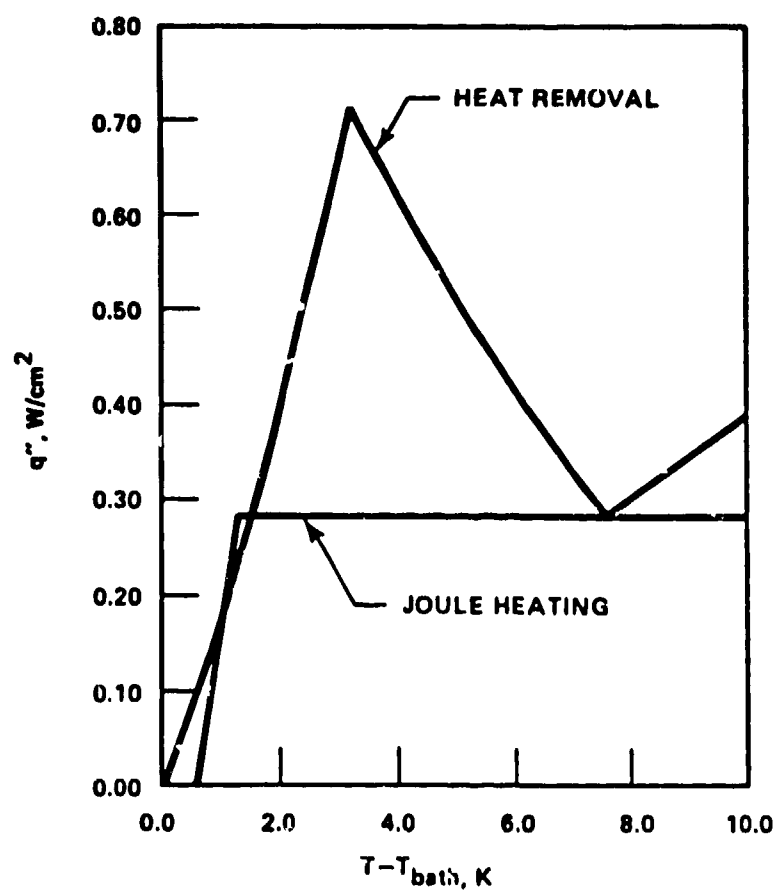
Coil Along

$\int_{0.60}^{1.46} \frac{\Delta P}{\Delta D} dD = 0.062 \text{ mJ} = 0.31\%$

Figure 3 - Minimum AC loss and ~~loss~~ loss distribution for a no second symmetrical higher order ~~mode~~ of the 20 MJ coil



4
 FIGURE 4 CONDUCTOR BEHAVIOR DURING A DIPOLAR PULSE



5
FIGURE 5 20 MJ CONDUCTOR STABILITY

TABLE 1
FINAL CONDUCTOR DESIGN

Operating Characteristics

Operating Current, I_{op} <i>5x10⁴ A/cm</i>	50,000 Amperes
I_{op}/i_c at 4.5 K, 7.5 T (<i>0.71</i>)	0.71
J_{op} (Circumscribed Conductor Area $t \times w$)	2,615 Amps/cm ²
Fully-normal Heat Transfer from 2/3 of Strand Surface	0.26 Watts/cm ²

Overall Cable Description

Conductor Length	677 meters*
Cable Dimensions	1.532 cm x 12.480 cm [†]
Configuration	Cable of Subcables
Number of Subcables, N	36
Mandrel Core Material	Nitronic 40
Mandrel Core Dimensions $t' \times w'$	0.211 cm x 11.164 cm
Mandrel Dimensions including Insulation, $t \times w$	0.257 cm x 11.210 cm
Cable Pitch Angle, θ	+18 Degrees
Cable Pitch Length and Sense, 4L	73 cm (plus angle)

Subcable Description

Configuration	Cable Around A Core
Number of Nb-Ti Strands, n	6
Subcable Diameter with Insulation, $2r_{sc}$	0.6374 cm
Core Strand Diameter with Insulation	0.2238
Pitch Length and Sense	4.670 cm (plus angle)
Core Strand Material	304 Stainless Steel
Core Strand Diameter Uninsulated, $2r_{sc}$	0.2187 cm
Insulation on Core Strands	Omega (Polyester Amide-Imide)
Core Strand Insulation Thickness	0.0025 cm

INTERMAGNETICS CORPORATION

TABLE 2-1 (Cont'd)
FINAL CONDUCTOR DESIGN AND PERFORMANCE

Subcable Description (Cont'd)

Nb-Ti Strand Overall Diameter $2r_1$	0.2068 cm
Nb-Ti Strand Insulation	Omega (Polyester Amide-Imide)
Nb-Ti Strand Insulation Thickness	0.0014 cm

* In the coil, 740 m delivered length.

† As confined under radial and axial compression in the winding.

INTERMAGNETICS GENERAL

TABLE 2

FINAL STRAND DESIGN

<u>Item</u>	<u>Value</u>
Metallic Radius*, r_s	1.020 mm (0.0402")
With Insulation, r_i	1.034 mm (0.0407")
Insulation Type	Omega (Polyester Amide-Imide)
Insulation Thickness	0.014 mm (0.0006")
Filament Region, r_f	0.600 mm (0.0236")
Fin Thickness, t_f	0.064 mm (0.0025")
Copper Shell, Δr	0.104 mm (0.0041")
Strand Twist, L_s	7.72 mm (0.304")
Cu Outer Area	7.825 mm^2 (3.02%)
Cu Core Area	8.633 mm^2 (3.32%)
Cu Total Area	2.474 mm^2 (7.64%)
90 Cu-10 Ni Area	0.335 mm^2 (10%)
Nb-Ti Area	8.476 mm^2 (45%)
Metal Within r_s	3.269 mm^2 (100%)
Filament Size, d	22.1 μm
# of Filaments, N_f	1,356
RRR Cu Between Filaments [†]	90
RRR Cu Elsewhere [†]	125
ρ_r , Cu-Ni	$17 \times 10^{-8} \Omega\text{m}$
Helium Within Conductor Envelope	43%
Fully Normal Heat From 2/3 Surface	0.26 Watts/cm ²

[†] 273 K to 4.2 K

Loss Type	Ref. #	Equations Used Equation	Loss For Coil Alone, % of 20 MJ	Loss As Part of Stack, % of 20 MJ
Transverse Field Strand Losses				
Coupling	()	$\frac{P_c}{V_{strand}} = \left(\frac{B_{\perp} L_s r_j}{2 \pi r_s} \right)^2 \left(\frac{1}{\rho_{\perp}} + \frac{\mu_{small}}{\rho_r} + \frac{\mu_{small}}{\rho_{Cu \text{ Outer}}} \right), \rho_{\perp} = \left(\frac{1+\lambda}{1-\lambda} \right) \rho_{Cu \text{ Core}}$	0.11	.15
Eddy Current	()	$\frac{P_e}{V_{strand}} = \frac{B_{\perp}^2}{4 \rho_{Cu \text{ Outer}}} \left[\frac{r_s^4 - (r_s - \Delta r)^4}{r_s^2 \text{ Shell}} + 6 \left(\frac{r_s}{r_s^2} \right) \right]_{small}$	0.07	.08
Hysteresis	()	$\frac{P_{ht}}{V_{strand}} = \frac{2 \lambda J_c d B }{3 \pi} g \left(\frac{I_{op}}{I_c} \right)$	0.04	.05
Transverse Field Strap Loss	()	$\frac{P_{ss}}{V_{ss}} = \frac{B_{\perp}^2 r_{ss}^2 V_{strand}}{4 \rho_{ss} V_{ss}} + \frac{B_{\perp}^2 (t^1)^2 V_{strap}}{12 \rho_{ss} V_{ss}} + \frac{B_{\perp}^2 (w^1)^2 V_{strap}}{12 \rho_{ss} V_{ss}}$	0.01	.00
Self-Field Hysteresis Loss	()	$\frac{Q_{sf}}{V_{strand}} = \frac{\nu_0 I_{op}^2}{4 \pi A_{strand}} \left[\frac{(2-F)F + 2(1-F)\ln(1-F)}{F^2} \right], F = \frac{I_{op}}{I_c}$	<0.06	<.06
Parallel Field Fully-Coupled Hysteresis Loss	()	$\frac{Q_{hp}}{V_{strand}} = \left[\frac{\pi^2 (r_f)^4}{6 \nu_0 r_s^2 L_s^2} \right] \left[\frac{(2 B_{11 \text{ max}})^3 B_c}{(2 B_{11 \text{ max}} + B_c)^2} \right], 2 B_{11 \text{ max}} < B_c$ $\frac{Q_{hp}}{V_{strand}} = \frac{K (2 B_{11 \text{ max}})^3}{4 B_c}, B_c < 2 B_{11 \text{ max}} < 2 B_c$ $\frac{Q_{hp}}{V_{strand}} = 6 K B_c (2 B_{11 \text{ max}} - 5/3 B_c), 2 B_{11 \text{ max}} > 2 B_c$ $B_c = \frac{\nu_0 \lambda J_c L_s}{4 \pi}, \text{ Parallel Filament Loss in } P_{ht}/V$	0.02	.03
Total Loss		Sum of Individual Losses	<0.31	<.37

TABLE 4.4

AFFECT OF HEAT TRANSFER AND COIL SIZE ON PERCENT LOSS
IN 50 KILOAMPERE CONDUCTORS USING THE 20 MJ STRAND DESIGN^A

B_{max} Coil (Tesla)	Heat Xfer (Watts/cm ²)	J_{op} 50 kAmp Conductor (Amp/cm ²)	Overall Coil J_{op} (Amp/cm ²)	A_{sc} / Strand (mm ²)	Strand Dia. (mm)	# of Strands (@ r)	I_{op}/I (4.5 K) cm	Bipolar Pulse and AC Loss (% of Coil Energy)
7.5, 20 MJ	1.26, 20 MJ Design	2,615	1,716	0.52	2.0	216	0.71	1 sec $\frac{1}{2}$ cos < 0.31
7.5, 20 MJ	0.36	3,138	2,059	0.52	2.0	180	0.86	1 sec $\frac{1}{2}$ cos < 0.26
7.5, 20 MJ	0.53	3,733	2,450	0.52	2.0	150	1.02	1 sec $\frac{1}{2}$ cos < 0.22
7.9 100 MJ [†]	0.36	3,071	2,015 [†]	0.52	2.0	174	1.06	1.8 sec ramp < 0.10
FOR COMPARISON, ANL 50 kAmp STRAND, I_{op} CONDUCTOR = 50,000 AMPS								
7.9 100 MJ	0.36 ^{††}	3,669*	2×10^3	0.53	2.5	144	1.00	1.8 sec ramp 0.16

* Does not include all of the stainless steel support.

† 100 MJ coil, assuming 20 MJ type of construction will be applicable for 100 MJoule.

†† IGC analysis and projection of minimum Nb-Ti content. Gives minimum Watts/cm².

RRR 150 in copper strands, RRR 60 in Nb-Ti strands assumed, ANL reported loss DOE Workshop 1/14/80.

^A Losses for coils operating alone (as opposed to in a stack).

INTERMAGNETICS